Electronic Supplementary Information

Surface Domain Heterojunction on Rutile TiO_2 for High-Efficient Photocatalytic Hydrogen Evolution

Kuo Lin,‡ Fang Xiao,‡ Ying Xie, Kai Pan, Lei Wang, Wei Zhou, and Honggang Fu**

Key Laboratory of Functional Inorganic Material Chemistry, Ministry of Education of the People's Republic of China, Heilongjiang University, Harbin, 150080, P. R. China

E-mail:zwchem@hotmail.com

fuhg@vip.sina.com

Characterizations

X-ray diffraction (XRD) patterns were obtained by a Bruker D8 Advance diffractometer by using Cu K_α radiation (λ = 1.5406 Å, 40 kV, 40 mA). The scan rate and the step size were 6 °/min and 0.02 °, respectively. Raman measurements were performed with a Jobin Yvon HR 800 micro-Raman spectrometer at 457.9 nm. The laser beam was focused with a 50 × objective lens to a ca. 1 μm spot on the surface of the sample. The surface morphology was measured by scanning electron microscopy (SEM, Hitachi S-4800, with an acceleration voltage of 5 kV) and transmission electron microscopy (TEM, JEOL

JEM-2100). X-ray photoelectron spectroscopy (XPS, Kratos, ULTRA AXIS DLD) was carried out with monochrome Al K_α ($h\nu$ = 1486.6 eV) radiation. All binding energies were calibrated by referencing to C 1s peak at 284.6 eV. UV-visible absorption spectroscopy was recorded using a UV-visible spectrophotometer (Shimadzu UV-2550). The band gaps were estimated by extrapolating a linear part of the plots to $(\alpha h\nu)^2 = 0$. Scanning Kelvin probe (SKP) measurements (SKP5050 system, Scotland) were performed at normal laboratory conditions. Surface photovoltage spectroscopy (SPS) measurements were carried out with a home-built apparatus equipped with a lock-in amplifier (SR830) synchronized with a light chopper (SR540). The photoluminescene spectra (PL) were recorded with a PELS 55 spectrofluoro-photometer with the excitation wavelength of 325 nm. The loading amount of Pt was according to Inductively Coupled Plasma (Optima 8300 (PerkinElmer, USA) ICP-OES). Fourier transform infrared spectroscopy (FT-IR) was recorded on a Perkin-Elmer Spectrum One spectrometer using KBr pellets. Nitrogen adsorption-desorption isotherms at 77 K were collected on an AUTOSORB-1 nitrogen adsorption apparatus. Surface area was estimated by Brunauer–Emmett–Teller (BET) method and pore-size distribution was measured from the adsorption branch of the isotherm using the Barrett-Joyner-Halenda (BJH) method. The positron annihilation experiments were carried out on EG&G ORTEC fast slow coincidence system with a resolution of 210 ps. The tablet was folded to surround the positron source (22Na, 5×10^5 Bq) with a total thickness of approximately 1 mm. The spectrum was resolved using the LTv9.0 software. Electron paramagnetic resonance

trapping measurement was as follows. 20 mg samples were dissolved in 5 ml DI water or methanol, then 50 μL solution was mixed with 500 μL 5,5-dimethyl-1-pyrroline-N-oxide (DMPO). After being illuminated for 15 s (Xe lamp with AM 1.5G), the mixture was characterized using a Brucker EMX plus model spectrometer operating at room temperature.

Water Contact Angle Measurement

Hydrophilicity was evaluated using a water contact angle (WCA) by static droplet method (sessile drop method), on a drop shape instrument (FTA1000, First Ten Angstroms). Immediately after preparation of the film (spray coating), 4 μL of distilled water was deposited on the specimen, and WCA after 10 s was measured by the curve fitting method of elliptic approximation.

Photocatalytic hydrogen evolution

The photocatalytic hydrogen evolution experiments were conducted in an online photocatalytic hydrogen generation system (AuLight, CEL-SPH2N, Beijing PerfectLight) at ambient temperature. Typically, 100 mg of the photocatalysts were dispersed in 100 mL of the mixed solution made of DI water and methanol (4:1). The suspension of photocatalysts was sealed in the closed-gas circulation reaction cell. Prior to the reaction, the mixture was deaerated by evacuation to remove O_2 and CO_2 dissolved in water. Subsequently, the actor was exposed under a 300 W Xe lamp (Oriel, USA). Gas evolution was observed under AM 1.5G irradiation with a power density of 100 mW cm^{-2}

and being analyzed by an on-line gas chromatograph (SP7800, TCD, molecular sieve 5 Å, N_2 carrier, Beijing Keruida Limited). The determination of the apparent quantum efficiency for hydrogen generation was performed using the same closed circulating system under illumination of a 300 W Xe lamp with bandpass filter (365 and 420 nm) system.

Photoelectrochemical test

Photoelectrochemical measurements were monitored by a CorrTest electrochemical station with a standard three-electrode system. The working electrodes were prepared by using samples coated on FTO glass. Pt plate and Ag/AgCl (saturated KCl) electrode were used as the counter electrode and reference electrode, respectively. The electrolyte was Na_2SO_4 solution (0.5 M) and purged with nitrogen for 3 h before measurement. All photoelectrochemical experiments were carried out under AM 1.5G irradiation.

The apparent quantum efficiency (AQY) and the solar-to-hydrogen (STH) efficiency

The apparent quantum efficiency (AQE) was calculated under different single-wavelength light using Equation (1):

$$\mathrm{AQE} = \frac{2 \times \text{the number of evolved } H_2 \text{ molecules}}{\text{then umber of incident photons}} \times 100\% \quad (1)$$

The solar to hydrogen (STH) conversion efficiency were calculated from the solar simulator measurements using Equation (2):

$$\mathrm{STH} = \frac{\text{output energy}}{\text{Energy of incidence solar light}} = \frac{r_{H_2} \Delta G}{P_{sun} \times S} \times 100\% \quad (2)$$

Turn-Over-Frequency (TOF) calculations

The TOF was calculated under AM 1.5G irradiation using Equation (3):

$$\mathrm{TOF} = \frac{\text{mole of evolved } H_2}{\text{mole of Pt atoms of catalyst} \times \text{reaction time}} \quad (3)$$

Density functional theory calculations

Density functional theory calculations were carried out by using the CASTEP code [S. J. Clark, M. D. Segall, C. J. Pickard, P. J. Hasnip, M. J. Probert, K. Refson, M. C. Payne, *Zeitschrift fuer Kristallographie*. **2005**, *220(5-6)*, 567]. Generalized Gradient Approximation (GGA) and Perdew-Wang functional (PW) [J. P. Perdew, Y. Wang, *Phys. Rev. B*. **1992**, *45*, 13244] were applied to deal with the exchange correlation energy. With the application of the ultra-soft pseudo-potential technique [D. Vanderbilt, *Phys. Rev. B*, **1990**, *41*, 7892-7895], the energy cut-off was set to 380 eV. A (4×4×1) grid was used when sampling over Brillouin zone. The (2×1×1) suppercell of TiO_2 (110) surface was constructed and depicted in **Scheme S1**. Geometry optimization was performance with the application of the Broyden-Fletcher-Goldfarb-Shanno algorithm (BFGS) [B. G. Pfrommer, M. Cote, S. G. Louie, M. L. Cohen, *J. Comput. Phys*. **1997**, *131*, 233-240] until the stress, the force, and the displacement on each atom were less than 0.02 Gpa, 0.01 $eV \cdot Å^{-1}$ and 5.0×10^{-4} Å, respectively. Under such conditions, the energy convergence of systems is restricted within 2.0×10^{-6} $eV \cdot atom^{-1}$. Furthermore, to evaluate the HER performance of the materials, the Gibbs adsorption energy of a single H atom on different

surfaces (ΔG_{H*}) was calculated according to Ref. [Y. Zheng, Y. Jiao, Y. Zhu, L. Li, Y. Han, Y. Chen, A. J. Du, M.Jaroniec, S. Qiao, *Nat. Commun.* **2014**, *5*, 3783; H. Yan, Y. Xie, A. Wu, Z. Cai, L. Wang, C. Tian, X. Zhang, H. Fu, *Adv.Mater*. **2019**, *31*, 1901174]. To avoid the pseudo-interaction between periodic images along z axis, a vacuum slab with the thickness of 15 Å was introduced.

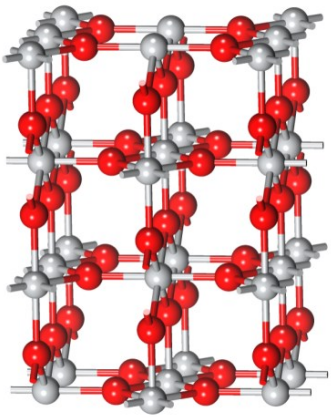

Scheme S1. Scheme of rutile TiO_2 (110) surface with (2×1×1) supercell.

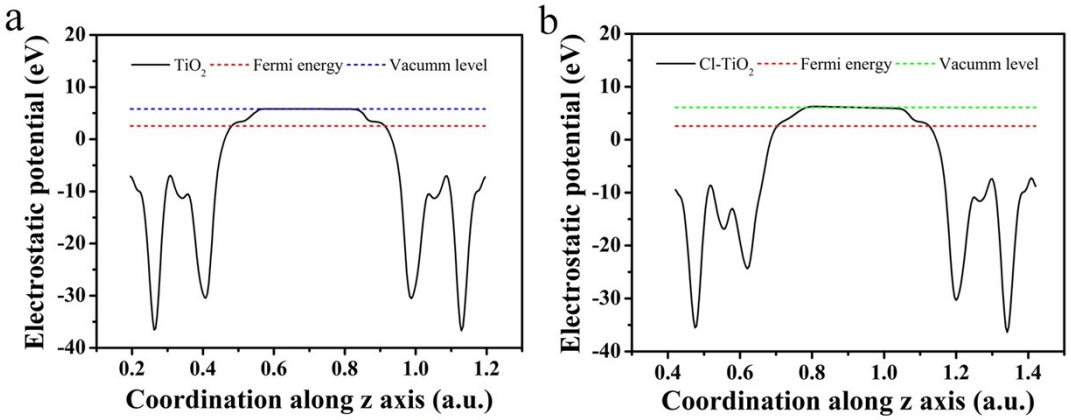

Figure S1. Average electrostatic potentials along z axis for rutile TiO_2 (a) and Cl-decorated rutile TiO_2 surface (b), respectively.

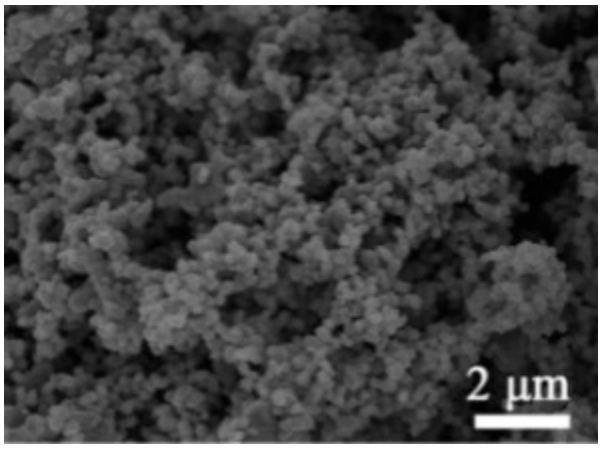

Figure S2. SEM image of titania oligomers particles as seeds.

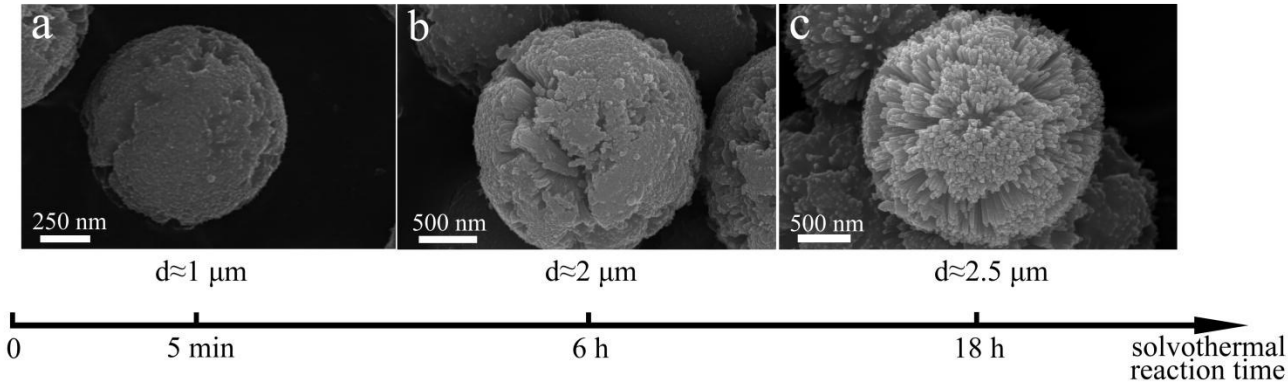

Figure S3. SEM images of the growth process of rutile TiO_2 microsphere at different reaction times: (a) 5 min; (b) 6 h; (c) 18 h.

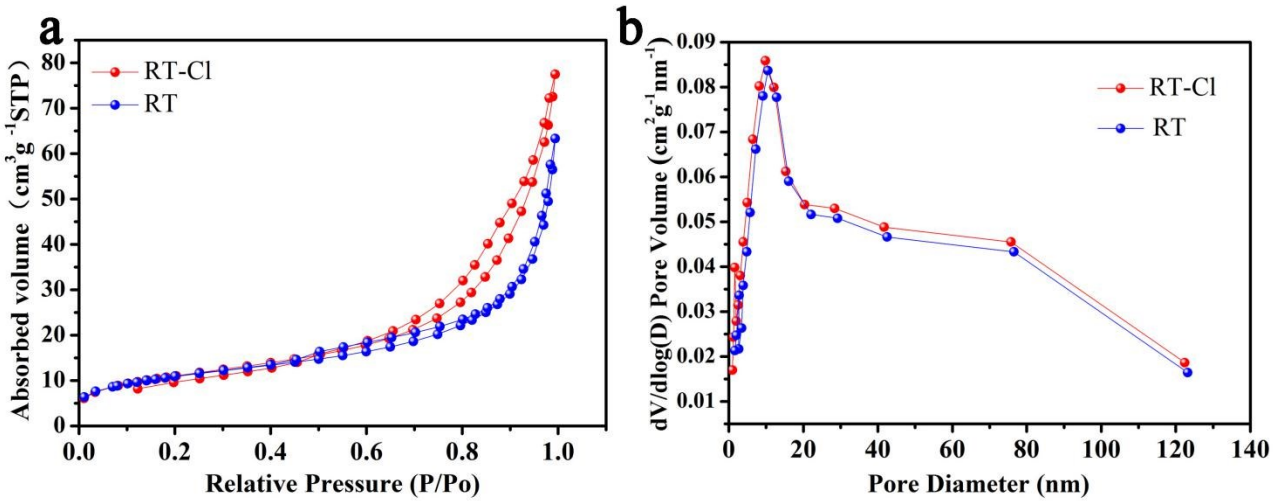

Figure S4. N_2 adsorption-desorption isotherms (a) and the corresponding pore size distributions (b) of RT and RT-Cl, respectively.

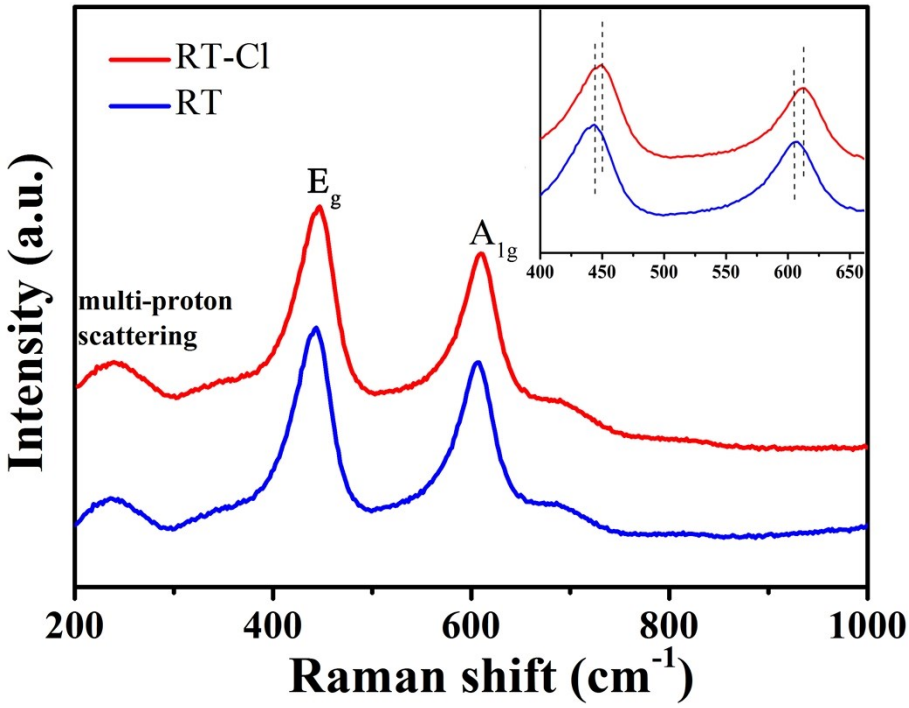

Figure S5. Raman spectra of RT and RT-Cl, respectively. The inset is the enlarged spectra between 400-660 cm^{-1}.

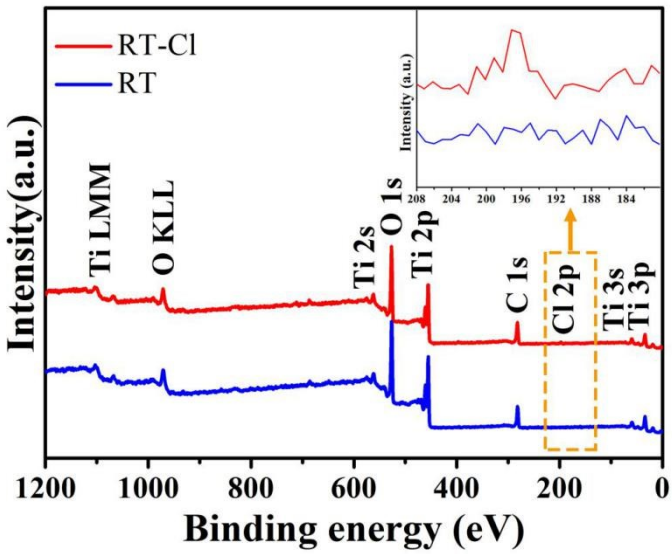

Figure S6. XPS survey spectra of RT and RT-Cl, respectively. The inset is the enlarged spectra between 180-208 eV.

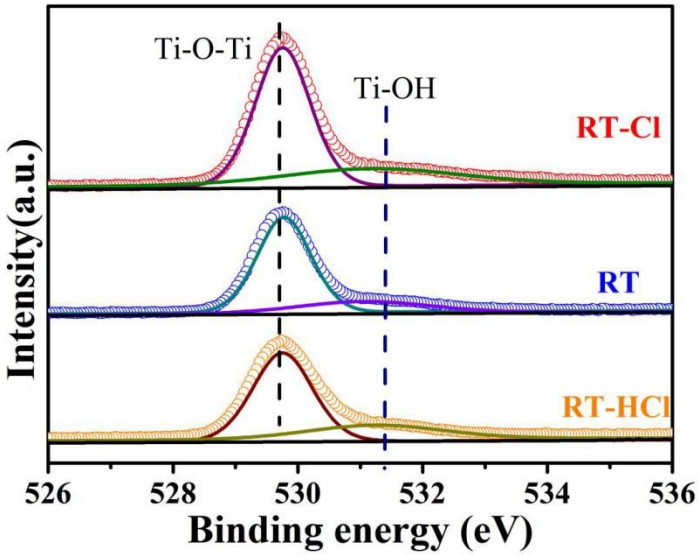

Figure S7. XPS spectra of O 1s for RT, RT-Cl and RT-HCl samples, respectively.

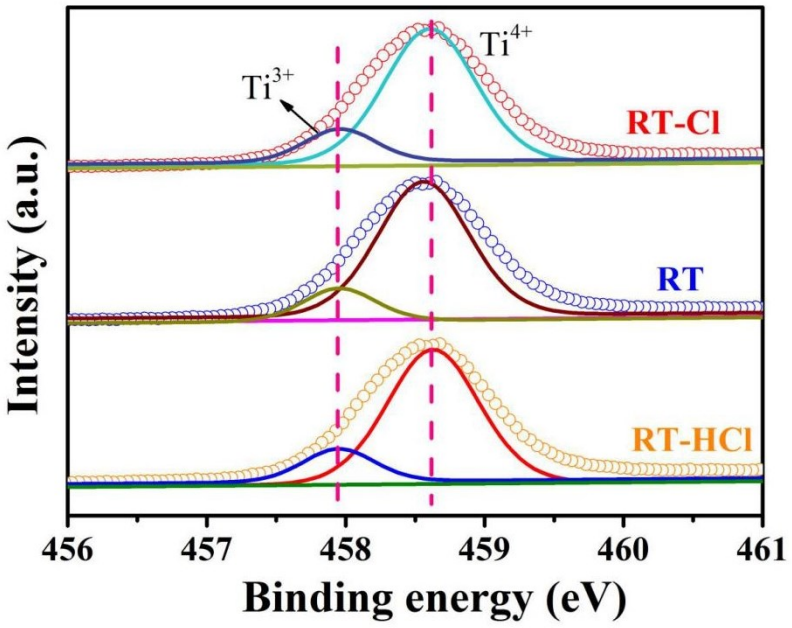

Figure S8. XPS spectra of Ti 2p for RT, RT-Cl and RT-HCl samples, respectively.

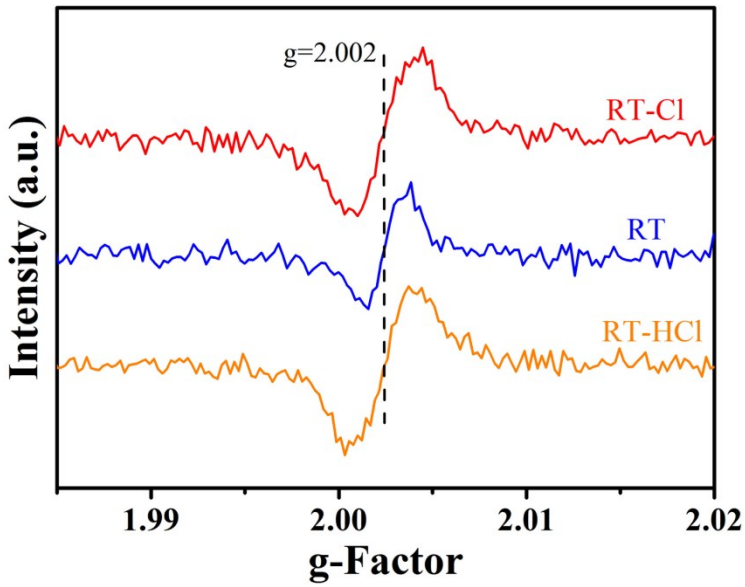

Figure S9. Electron paramagnetic resonance spectra of RT-Cl, RT, and RT-HCl, respectively.

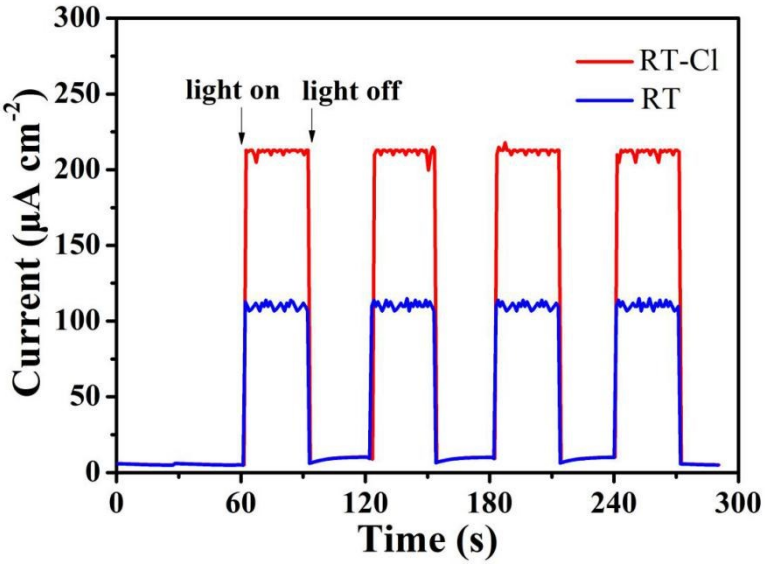

Figure S10. Chronoamperometry responses of RT and RT-Cl, respectively.

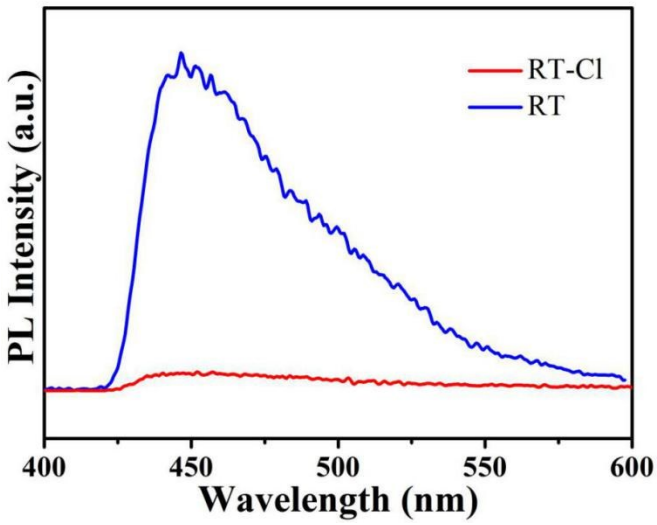

Figure S11. PL spectra of RT and RT-Cl, respectively.

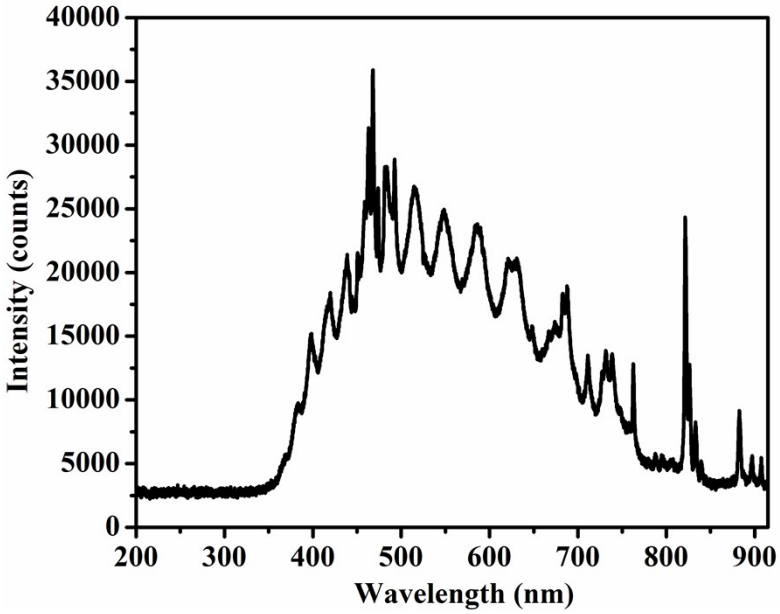

Figure S12. The UV-vis spectrum of solar simulator equipped with an AM 1.5G filter.

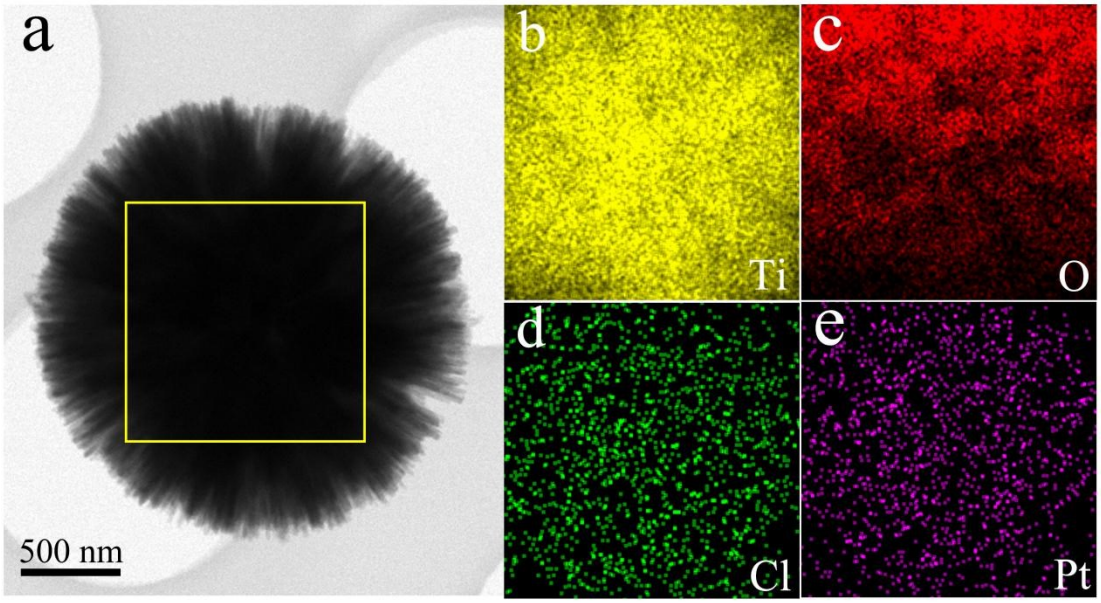

Figure S13. The TEM image (a) and the corresponding EDX mapping images of elemental Ti (b), O (c), Cl (d), and Pt (e) in the selected area in panel of RT-Cl.

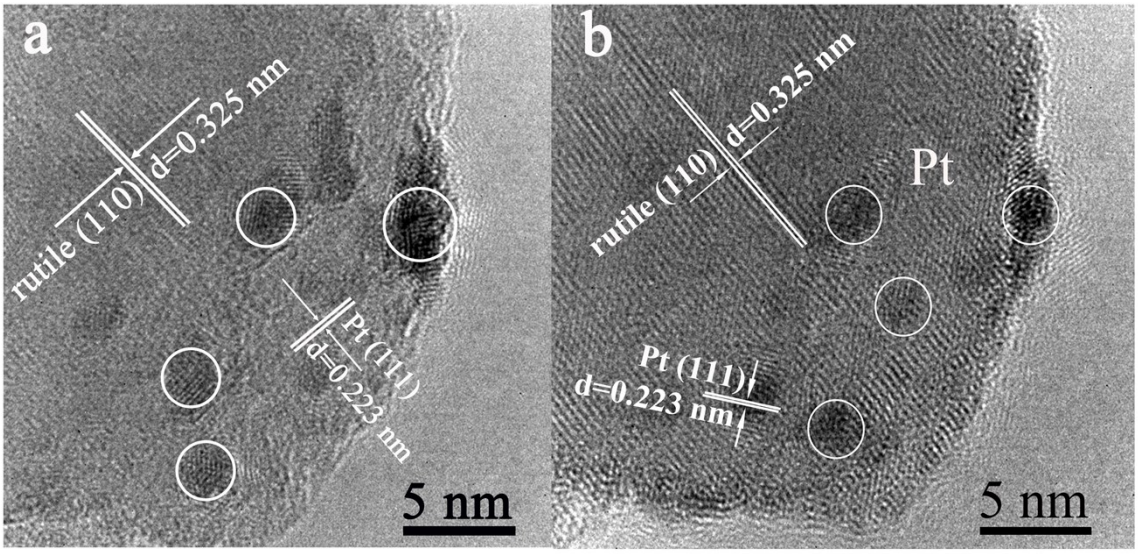

Figure S14. HRTEM images of RT (a) and RT-Cl (b) with Pt nanoparticles as co-catalyst (the main diameter of 2~3 nm).

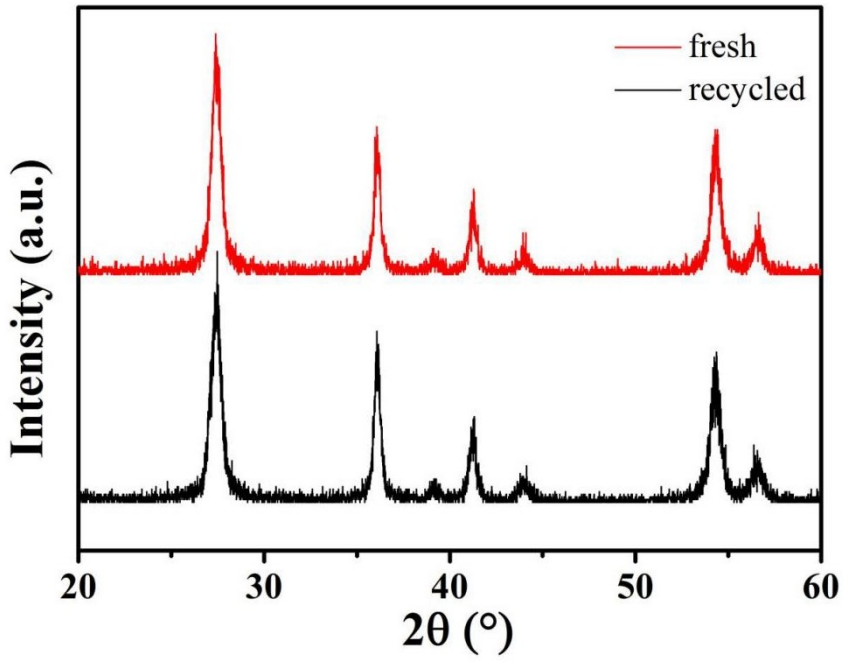

Figure S15. XRD patterns of fresh sample (RT-Cl) and the sample after 5 recycles.

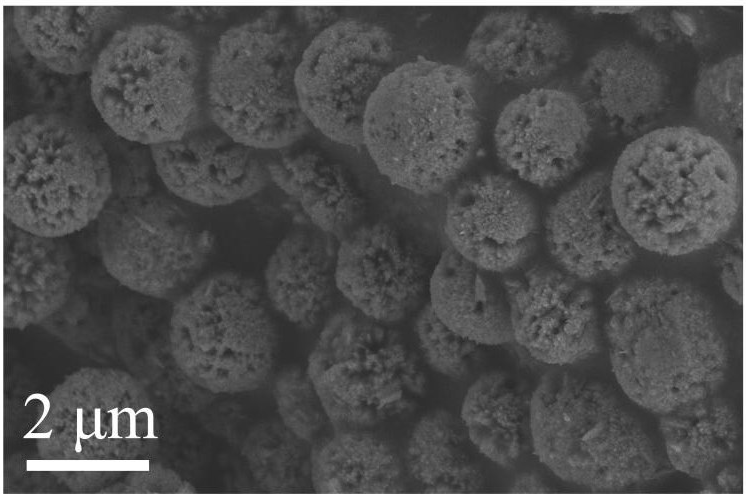

Figure S16. SEM image of the RT-Cl sample after 5 recycles.

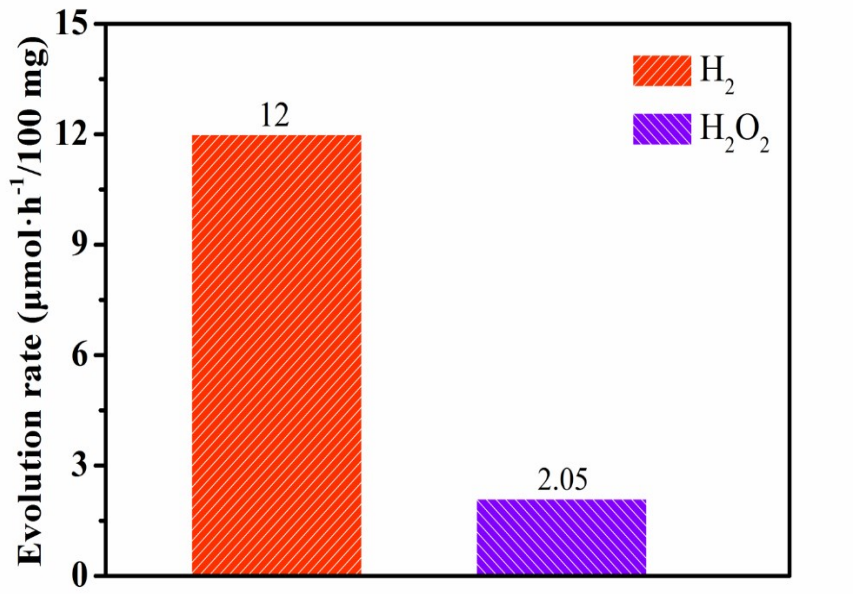

Figure S17. H_2 and H_2O_2 evolution rates of RT-Cl sample for pure water splitting.

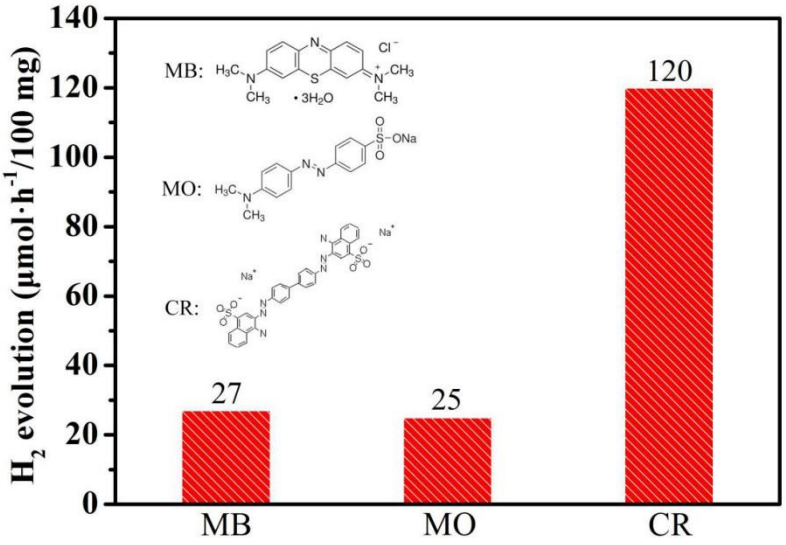

Figure S18. Photocatalytic hydrogen evolution of RT-Cl in Methylene Blue (MB), Methyl Orange (MO), and Congo Red (CR) aqueous solutions (20 mg L^{-1}).

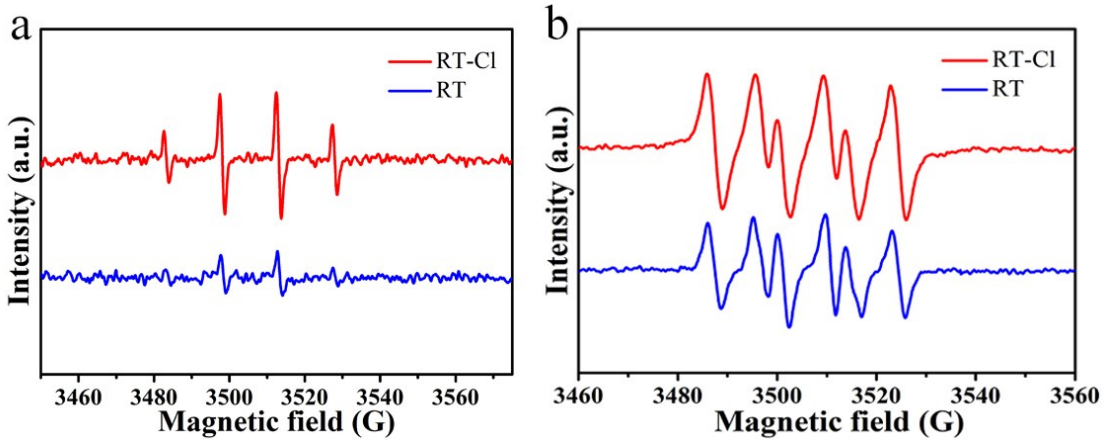

Figure S19. EPR spectra in the presence of DMPO in water (a) and in CH_3OH (b), respectively.

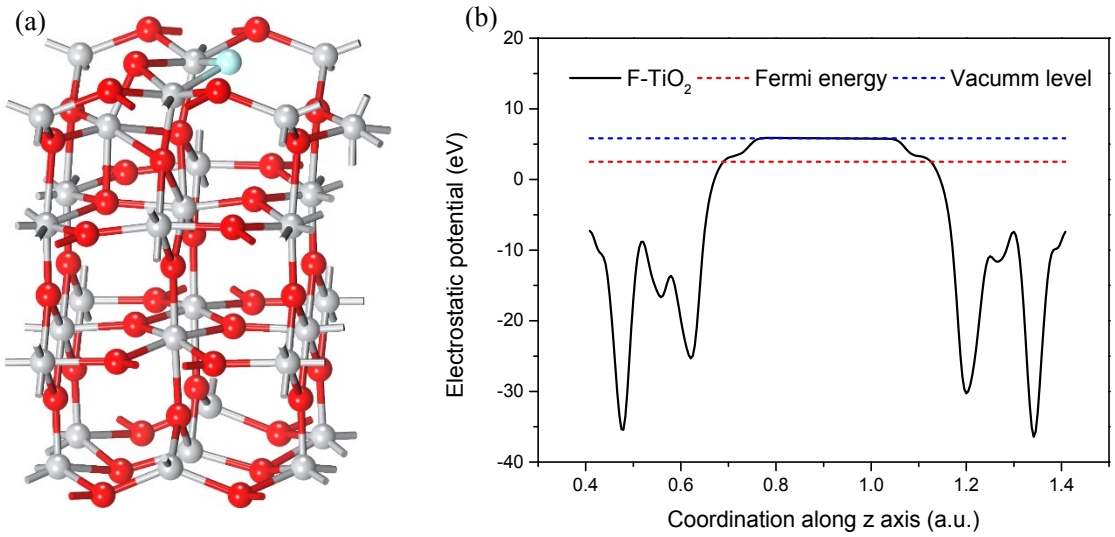

Figure S20. Optimized structure for F-decorated rutile TiO_2 surface (a) and the electrostatic potential along z axis (b).

To clarify whether the SDH mechanism is applicable or not for F-decorated rutile TiO_2, additional calculations are performed. The results suggest that the work function for F-decorated rutile TiO_2 is 3.309 eV, which is very close to the value (3.241 eV) for pure rutile TiO_2. As a result, the bottom of the conduction band of F-decorated rutile TiO_2 should be lower than that of ideal rutile TiO_2 by about 0.068 eV. Although this value is small, the SDH mechanism should be also applicable for F-decorated rutile TiO_2.

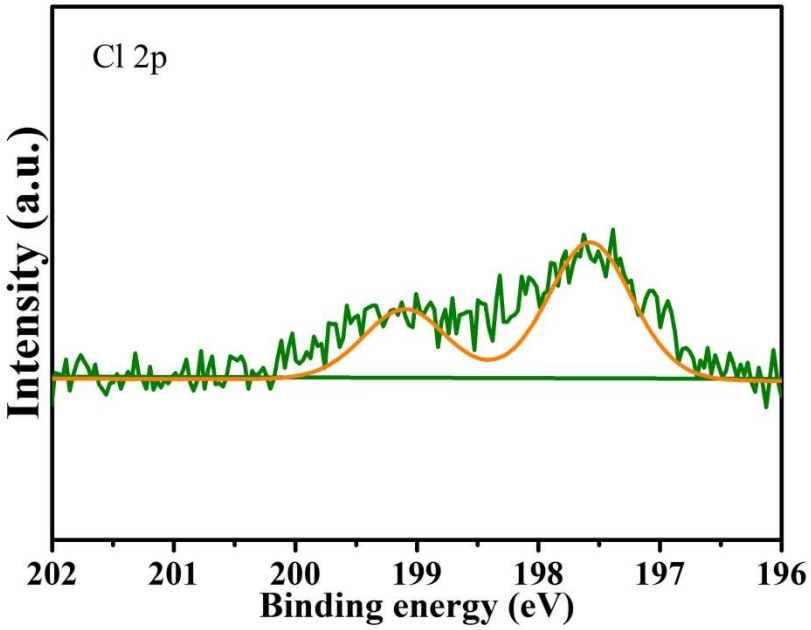

Figure S21. XPS spectrum of Cl 2p for RT-HCl.

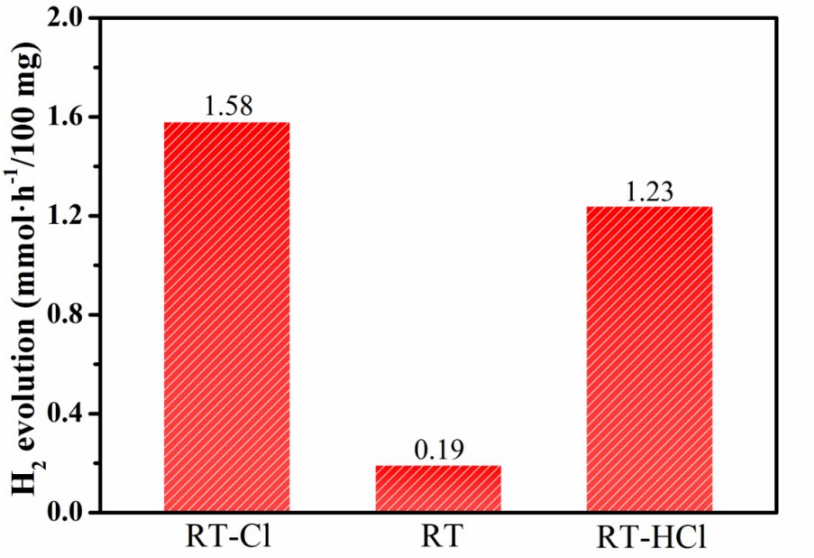

Figure S22. Photocatalytic hydrogen rates of RT, RT-Cl and RT-HCl samples, respectively.

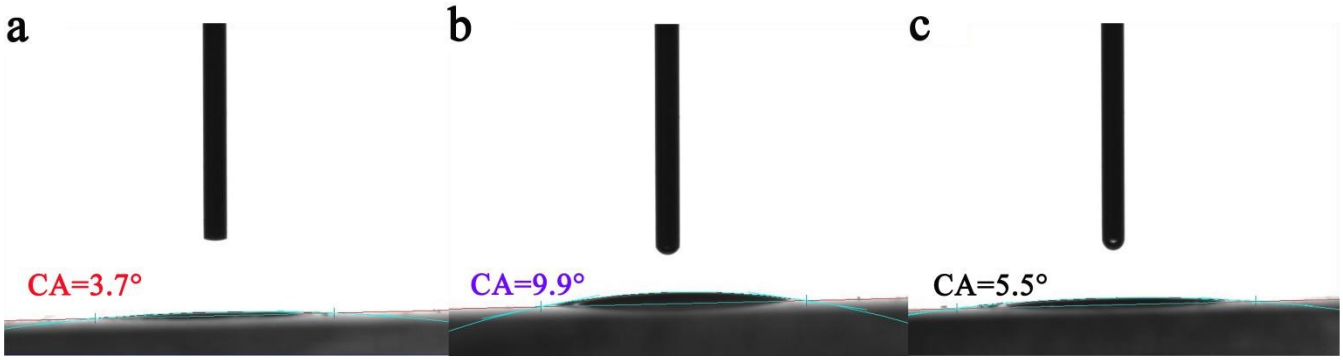

Figure S23. Water contact angles (CA) of RT-Cl (a), RT (b) and RT-HCl (c) samples, respectively.

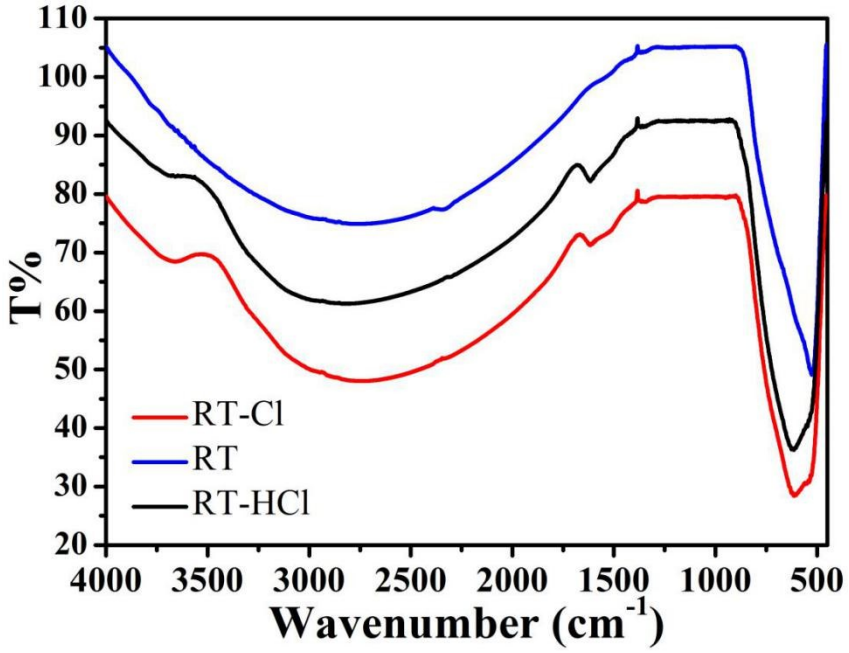

Figure S24. FT-IR spectra of RT, RT-Cl and RT-HCl, respectively.

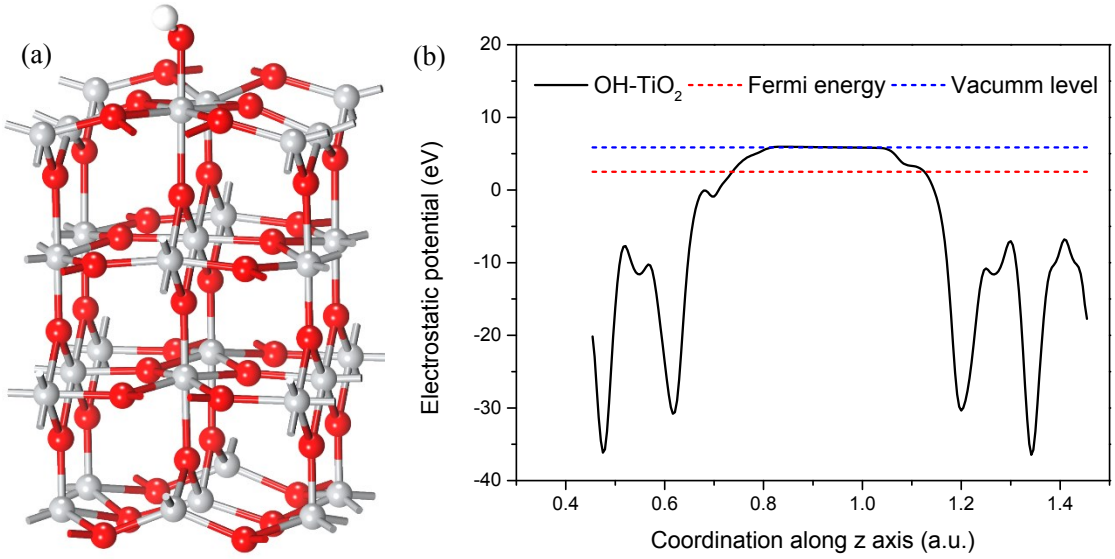

Figure S25. Optimized structure for OH-decorated rutile TiO_2 surface (a) and the electrostatic potential along z axis (b).

To evaluate the effect of hydroxyl group on the band alignment of the system, additional calculations were further performed. It shows the optimized structure with the decoration of hydroxyl group. The work function of this system is calculated to be 3.354 eV. Although this value is slightly larger than that of pure rutile TiO_2 (3.241 eV), a large step (0.182 eV) between OH-decorated and Cl-decorated TiO_2 components is still remained. Therefore, the introduction of OH group should not affect the present results.

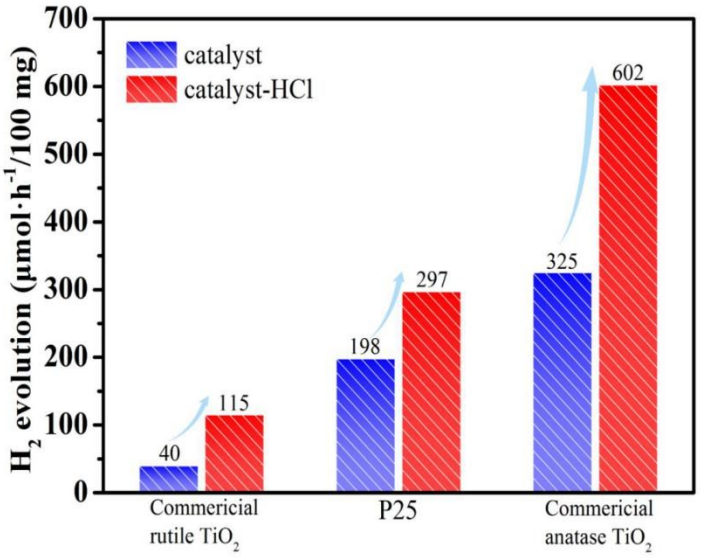

Figure S26. Comparison of hydrogen evolution rate (AM 1.5G) for different commercial photocatalysts with (Catalyst-HCl) and without (Catalyst) HCl hydrothermal reaction.

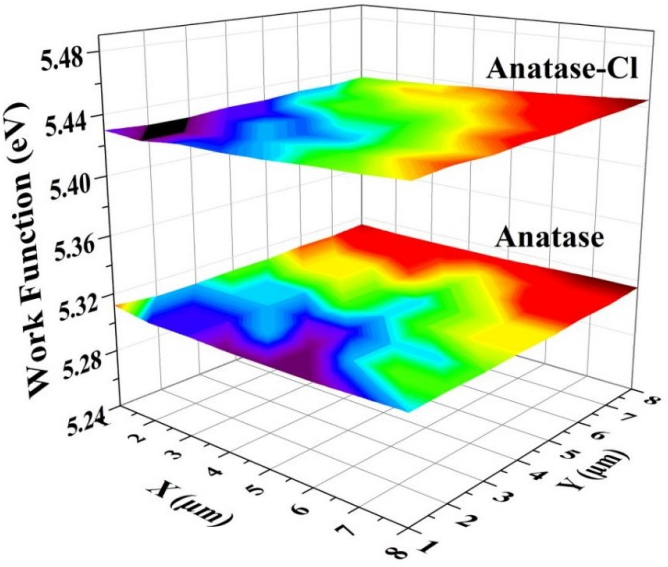

Figure S27. SKP maps of anatase TiO_2-Cl and pure anatase TiO_2.

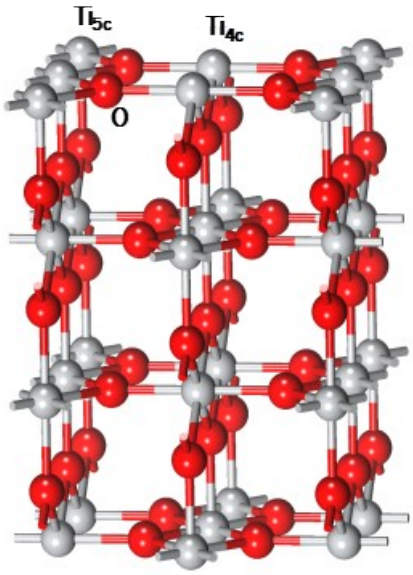

Figure S28. Scheme of 4-coordinated Ti (Ti_{4c}) and 5-coordinated Ti sites (Ti_{5c}) for ideal rutile TiO_2 (110) surface.

Table S1. The lattice parameters and structure parameters of RT and RT-Cl.

parameters	RT-Cl	RT
Lattice constant (Å)	a=b=4.5882 c=2.9568	a=b=4.5790 c=2.9592
Cell volume ($Å^3$)	62.2453	62.0463
BET surface area ($m^2 g^{-1}$)	39.3	38.3
Pore size (nm)	10.9	11.2
Pore volume ($cm^3 g^{-1}$)	0.10	0.11

Table S2. Apparent quantum efficiency for different samples.

	365 nm	420 nm	520 nm
RT-Cl	75.2%	9.40%	1.24%
RT	9.01%	1.12%	0.14%
RT-HCl	60.9%	7.60%	0.96%

Table S3. Comparison of different rutile TiO_2 photocatalysts for hydrogen evolution.

Photocatalysts	H_2 activity ($\mu mol \cdot h^{-1}$/100 mg)	Light source	Reaction system	References
Rutile TiO_2	536.6	UV-vis	10% CH_3OH	[1]
Rutile TiO_2	144	UV	10% CH_3OH	[2]
Rutile TiO_2	115	Xe lamp,300 W	20% CH_3OH	[3]
Rutile TiO_2	270	Xe lamp,300 W	20% CH_3OH	[4]
Rutile TiO_2	331	400<λ<625 nm	20% CH_3OH	[5]
Rutile TiO_2	770	UV	50% CH_3OH	[6]
Rutile TiO_2	460	Xe lamp,300 W	20% CH_3OH	[7]
Rutile TiO_2	215.7	Xe lamp,300 W	20% CH_3OH	[8]
Rutile TiO_2	18.1	λ>400 nm	25% CH_3OH	[9]
Rutile TiO_2	140	λ>420 nm	20% CH_3OH	[10]
Rutile TiO_2	1200	Xe lamp,300 W	20% CH_3OH	[11]
Rutile TiO_2	900	Xe lamp,300 W	30% CH_3OH	[12]
Rutile TiO_2	245	λ>400 nm	40% CH_3OH	[13]
Rutile TiO_2	160	Xe lamp,300 W	1 M CH_3OH	[14]
Rutile TiO_2	600	Xe lamp,300 W	20% CH_3OH	[15]

Rutile TiO_2	250	AM 1.5G	50% CH_3OH	[16]
Rutile TiO_2	**1590**	**AM 1.5G**	**20% CH_3OH**	**This work**

References

[1] Y. Yang , G. Liu , T. S. John, H. Cheng, *Adv. Mater.* **2016**, *28*, 5850.

[2] C. Gao, T. Wei, Y. Zhang, X. Song, Y. Huan, H. Liu, M. Zhao, J. Yu, X. Chen, *Adv. Mater.* **2019**, *31*, 1806596.

[3] Y. Zhang, Z. Xu, G. Li, X. Huang, W. Hao,Y. Bi, *Angew. Chem. Int. Ed*. **2019**, *58*, 14229.

[4] H. Xiong, L. Wu, Y. Liu, T. Gao, K. Li, Y. Long, R. Zhang, L. Zhang, Z. Qiao, Q. Huo, X. Ge, S. Song, H. Zhang, *Adv. Energy Mater*. **2019**, 1901634.

[5] T. D. Phan, S. Luo, D. Vovchok, J. Llorca, J. Graciani, J. F. Sanz, S. Sallis, W. Xu, J. Bai, F. J. Piper, D. E. Polyansky, E. Fujita, S. D. Senanayake, D. J. Stacchiola, J. Rodriguez, *ACS Catal*. **2016**, *6*, 407.

[6] F. Amano, M. Nakata, Y. Akira, T. Tanakabc, *Catal. Sci. Technol.* **2016**, *6*, 5693.

[7] Q. Xu, Y. Ma, J. Zhang, X. Wang, Z. Feng, *J. Catal.* **2011,** *278***,** 329.

[8] Q. Zhang, R. Li, Z. Li, A. Li, S. Wang, Z. Liang, S. Liao, C. Li, *J. Catal.* **2016**, *337*, 36.

[9] F. Zuo, K. Bozhilov, R. J. Dillon, L. Wang, P. Smith, X. Zhao, C. Bardeen, P. Feng, *Angew. Chem. Int. Ed.* **2012**, *51*, 6223.

[10] Z. Zhao, H. Tan, H. Zhao, Y. Lv, L. Zhou, Z. Sun, *Chem. Commun*. **2014**, *50*, 2755.

[11] R. Li, Y. Weng, X. Zhou, X. Wang, Y. Mi, R. Chong, H. Han, C. Li, *Energy Environ. Sci.* **2015**, *8*, 2377.

[12] X. Zheng, Q. Kuang, K. Yan, Y. Qiu, J. Qiu, S. Yang, *ACS Appl. Mater. Interfaces*. **2013**, *5*, 11249.

[13] Y. Yang, Y. Yao, L. He, Y. Zhong, Y. Ma, J. Yao, *J. Mater. Chem. A*. **2015**, *3*, 10060.

[14] R. J. Ramalingam, T. Radhika, P. R. Ranjan, R. M. Sayed, H. A. Al-lohedan, A. M.

Moydeen, D. M. Al-dhayan, *Int. J. hydrogen energy* **2019**, *44,* 23959.

[15] W. Jiao, Y. Xie, R. Chen, C. Zhen, G. Liu, X. Ma, H. Cheng, *Chem. Commun.* **2013**, *49*, 11770.

[16] N. Y. Kim, H. K. Lee, J. T. Moon, J. B. Joo, *Catalysts* **2019**, *9*, 491.

Table S4. Comparison of hydrogen evolution for different Pt loading amounts on TiO_2.

Photocatalysts	Pt loading amounts (wt%)	H_2 activity ($\mu mol \cdot h^{-1}$/100 mg)	Light source	Reaction system	References
Rutile-Anatase TiO_2	0.6	1000	AM 1.5G	50% CH_3OH	[1]
Rutile TiO_2	1	400	Xe lamp,300 W	10% CH_3OH	[2]
Rutile TiO_2	1	181	λ>400 nm	25% CH_3OH	[3]
Rutile TiO_2	0.5	258	AM 1.5G	25% CH_3OH	[4]
Anatase TiO_2	3	750	AM 1.5G	20% CH_3OH	[5]
Degussa P25	1	561	Uv-vis	10% CH_3OH	[6]
Anatase TiO_2	0.6	845	Xe	20%	[7]

			lamp,300 W	CH_3OH	
Anatase TiO_2	0.54	217	Xe lamp,300 W	10% TEOA	[8]
Anatase TiO_2	0.5	811	Xe lamp, λ=420 nm	20% CH_3OH	[9]
Rutile-Anatase TiO_2	1	420	Xe lamp,300 W	10% CH_3OH	[10]
Rutile TiO_2	**0.15**	**1590**	**AM 1.5G**	**20% CH_3OH**	**This work**

References

[1] X. Chen, L. Liu, P. Y. Yu, S. S. Mao, *Science* **2011**, *331*, 746.

[2] L. Li, J. Yan, T. Wang, Z. Zhao, J. Zhang, J. Gong, N. Guan, *Nat. Commun*. **2015**, *6*, 5881.

[3] F. Zuo, K. Bozhilov, R. J. Dillon, L. Wang, P. Smith, X. Zhao, C. Bardeen, P. Feng, *Angew. Chem. Int. Ed*. **2012**, *124*, 6223.

[4] C. Yang, Z. Wang, T. Lin, H. Yin, X. Lv, D. Wan, T. Xu, C. Zheng, J. Lin, F. Huang, X. Xie, M. Jiang, *J. Am. Chem. Soc*. **2013**, *135*, 17831.

[5] O. Elbanna, M. Zhu, M. Fujitsuka, T. Majima, *ACS Catal.* **2019**, *4*, 3618.

[6] L.Ye, K. H. Chu, B. Wang, D. Wu, H. Xie, G. Huang, H. Y. Yipa, P. K. Wong, *Chem. Commun*. **2016**, *52*, 11657.

[7] Y. Sui, S. Liu, T. Li , Q. Liu, T. Jiang, Y. Guo, J. Luo, *J. Catal.* **2017**, *353*, 250.

[8] X. Tan, J. Zhang, D. Tan, J. Shi, X. Cheng, F. Zhang, L. Liu, B. Zhang, Z. Su, B. Han, *Nano Res*. **2019**, *12*, 1967.

[9] Y. Yang, P. Gao, X. Ren, L. Sha, P. Yang, J. Zhang, Y. Chen, L. Yang, *Appl. Catal. B:Environ.* **2017**, *218*, 751.

[10] X. An, C. Hu, H. Liu, J. Qu, *Langmuir* **2018**, *34*, 1883.

Table S5. Positron Lifetime Parameter of the rutile TiO_2 catalysts.

Sample	τ_1 (ps)	τ_2 (ps)	τ_3 (ps)	I_1 (%)	I_2 (%)	I_3 (%)
RT-Cl	111.6±5.7	332.2±2.0	974±84	12.86±0.55	85.90±0.58	1.24±0.23
RT	133.0±11	340.7±7.4	706±48	19.20±1.60	75.70±1.80	5.10±1.30

Table S6. Comparison of hydrogen evolution for different halogen decorated RT photocatalysts under AM 1.5G.

Photocatalysts	H_2 evolution ($\mu mol \cdot h^{-1}$/100 mg)	Increased ratio
RT	190	—
RT-F	332	75%
RT-Br	284	49%
RT-I	243	28%

Table S7. Comparison of hydrogen evolution for different surface chlorine amounts on RT-HCl.

HCl concentration (mol/L)	Surface chemisorbed chlorine amounts (%)	H_2 activity ($mmol \cdot h^{-1}$/100 mg)
0.1	0.18	0.48
0.2	0.33	0.92
0.3	0.47	1.23
0.4	0.47	1.23